Non-Hermitian squeezed polarons

Fang Qin (覃昉) [*], Ruizhe Shen, and Ching Hua Lee [†]

Department of Physics, National University of Singapore, Singapore 117542, Singapore

Recent experimental breakthroughs in non-Hermitian ultracold atomic lattices have dangled tantalizing prospects in realizing exotic, hitherto unreported, many-body non-Hermitian quantum phenomena. In this work, we propose and study an experimental platform for a radically different non-Hermitian phenomenon dubbed polaron squeezing. We find that it is marked by a dipolelike accumulation of fermions arising from an interacting impurity in a background of non-Hermitian reciprocity-breaking hoppings. We computed their spatial density and found that, unlike Hermitian polarons which are symmetrically localized around impurities, non-Hermitian squeezed polarons localize asymmetrically in the direction opposite to conventional non-Hermitian pumping and nonperturbatively modify the entire spectrum, despite having a manifestly local profile. We investigated their time evolution and found that, saliently, they appear almost universally in the long-time steady state, unlike Hermitian polarons which only exist in the ground state. In our numerics, we also found that, unlike well-known topological or skin localized states, squeezed polarons exist in the bulk, independently of boundary conditions. Our findings could inspire the realization of many-body states in ultracold atomic setups, where a squeezed polaron can be readily detected and characterized by imaging the spatial fermionic density.

Introduction. Rapid recent experimental progress in metamaterial [1–8], circuit [9–16], photonic [17–23], and ultracold atomic [24–29] realizations of non-Hermitian models have made unconventional features such as exceptional branch points [30–38] and non-Hermitian topological windings [39–46] experimental realities. However, to date, their explorations have mostly been confined to the single-body paradigm, with associated phenomena such as gapped topological transitions [47,48], unconventional criticality [49], negative entanglement entropy [50–52], and the breakdown of bulk-boundary correspondences [53–65]. But even more intriguing, many-body phenomena have come within the horizon ever since the very recent experimental breakthroughs in non-Hermitian ultracold atomic setups [24–29]. The interplay of non-Hermiticity with many-body effects has now become a possibility, as captured by emerging directions such as non-Hermitian many-body localization [66–69], superfluids [70–75], and Fermi liquids [76–84].

In this work, through exact diagonalization computations [85,86], we discover a non-Hermitian many-body phenomenon dubbed "polaron squeezing," which is a directional dipolelike accumulation effect arising from the triple interplay of impurity interactions, fermionic statistics, and non-Hermitian flux. In conventional Hermitian settings, polarons are many-body states dressed by the environment-impurity interaction, as observed in ultracold-atom experiments involving both fermions [87–95] and bosons [96–98]. By providing a unique angle for understanding strong interactions in solid-state and cold-atom systems, they are valuable probes for

detecting quantum phase transitions in interacting topological settings [99–105].

Going beyond well-understood Hermitian polarons [105–128], we found that, with non-Hermiticity and flux, polarons can acquire interesting aggregate behavior, with chiral delocalizing tendencies competing with impurity localization, in a way distinct from noninteracting impurities under the non-Hermitian skin effect (NHSE) [129]. Fermion degeneracy pressure introduces another level of intrigue by enforcing a special type of equilibrium among these competing influences. The result is a unique real-space "squeezed" fermionic density profile that, as we show, can be feasibly imaged in a realistic ultracold atomic demonstration.

Arising from predominantly many-body mechanisms, squeezed polaron states are distinct from other existing well-known types of robust states in related physical settings. Chiral topological states [130,131] [Fig. 1(a)], for instance, are edge localized and asymmetrically propagating, but they originate from nontrivial Chern topology, which is already completely well-defined in the single-particle context. Non-Hermitian boundary-localized skin states [53–59] [Fig. 1(b)] are also essentially single-particle phenomena, with their robustness stemming from the directed non-Hermitian "pumping" in nonreciprocal lattices. In contrast, squeezed polarons [Fig. 1(c)] are bona fide many-body states localized beside an impurity *interacting* with the fermions, and they can exist without nontrivial topology or physical boundaries. Due to their many-body nature, squeezed polarons also exhibit spatial profiles that are very different from those of topological or skin states.

Squeezed polarons from interactions and nonreciprocal gain and loss. To understand the primary mechanism behind polaron squeezing, we first examine a minimal toy model $\hat{H}_{\min}$

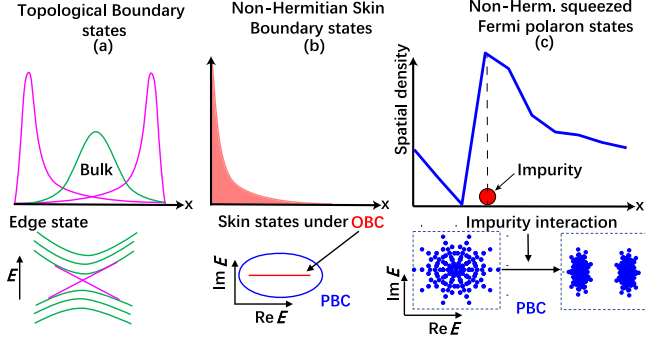[*] qinfang@nus.edu.sg
[†] phylch@nus.edu.sg

FIG. 1. Non-Hermitian polaron squeezing is distinct from other mechanisms for localized states, such as (a) topological localization and (b) the non-Hermitian skin effect, both single-body mechanisms requiring open boundaries. By contrast, squeezed polarons (c) are special asymmetric dipolelike accumulations across either side of an interacting impurity. They are many-body dressed states in the bulk, with charge density "squeezed" in the opposite direction from non-Hermitian pumping. Illustrative numerics are from $\hat{H}_{\min}$ of Eq. (1).

where fermions interact with a single impurity with strength g and hop asymmetrically with amplitudes $e^{\pm\alpha}$ around a ring with circumference L that gives periodic boundary conditions (PBCs):

$$\hat{H}_{\min} = g\hat{b}^{\dagger}_{x_0}\hat{b}_{x_0}\hat{c}^{\dagger}_{x_0}\hat{c}_{x_0} + \sum_x (e^{\alpha}\hat{c}^{\dagger}_x\hat{c}_{x+1} + e^{-\alpha}\hat{c}^{\dagger}_{x+1}\hat{c}_x). \quad (1)$$

Here $\hat{c}$ and $\hat{b}$ are respectively the second-quantized operators for the fermions and the impurity, which is fixed at an arbitrary site x_0. They experience a density-density interaction of strength g. The fermions also experience asymmetric hoppings $e^{\pm\alpha}$, which are the simplest possible terms that represent the simultaneous breaking of Hermiticity and reciprocity [132]. Importantly, due to the PBCs, these asymmetric hoppings cannot be "gauged away" as in conventional literature on the boundary accumulation of non-Hermitian skin states [53,55]. This independence from boundary accumulation is the first hint of the fundamental distinction between squeezed polarons and topological as well as skin states.

Squeezed polarons arise when the two parameters g and α of $\hat{H}_{\min}$ are both nonzero and sufficiently large. To elucidate their behavior, we turn on g and α under PBCs and observe how that affects the energy spectrum and long-time steady-state spatial density

$$\rho(x) \equiv \lim_{t\to\infty} \langle \psi^R(t) | \hat{c}^{\dagger}_x\hat{c}_x | \psi^R(t) \rangle. \quad (2)$$

Here $|\psi^R(t)\rangle = e^{-i\hat{H}t}|\psi^R(0)\rangle / \|e^{-i\hat{H}t}|\psi^R(0)\rangle\|$ is the normalized N-fermion right eigenstate that has time evolved from a specified initial state $|\psi^R(0)\rangle$. This evolution is taken over a sufficiently long time t, such that the spatial density approaches a steady spatial configuration.

When $\alpha = g = 0$ [Figs. 2(a1) and 2(a2)], we trivially have Hermitian nearest-neighbor hoppings with a real gapless spectrum. Due to translation invariance from PBCs, $\rho(x) = 0.5$ everywhere. Turning on the impurity interaction such that $\alpha = 0$ and $g = -100$ [Figs. 2(b1) and 2(b2)], we realize a minimal Hermitian polaron bound state, with $\rho(x)$ peaking at the impurity x_0. It is the polaron bound by the gap which
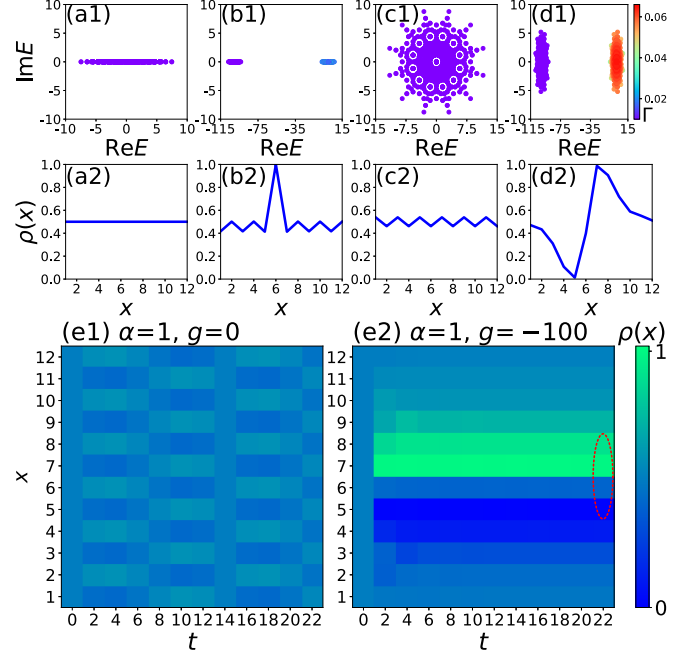

FIG. 2. PBC spectrum E [panels (a1)–(d1)] and spatial density $\rho(x)$ [panels (a2)–(d2)] for $\hat{H}_{\min}$ [Eq. (1)] with different nonreciprocities α and impurity interaction strengths g: (a1, a2) $\alpha = g = 0$; (b1, b2) $\alpha = 0$, $g = -100$; (c1, c2) $\alpha = 1$, $g = 0$; and (d1, d2) $\alpha = 1$, $g = -100$. Energy eigenstates $|\psi\rangle$ are colored by their squeezing asymmetric parameter Γ, which captures polaron squeezing: Γ is large only with both nonreciprocity and impurity interaction (d1). While the spatial polaron density $\rho(x)$ is symmetrically peaked about the impurity at $x_0 = 6$ when Hermitian (b2), it is asymmetrically squeezed in the non-Hermitian case (d2). (e1, e2) Dynamics of the spatial density for (e1) $\alpha = 1$, $g = 0$ and for (e2) $\alpha = 1$, $g = -100$, with the dipolelike asymmetric profile as circled. All computations are with $N = 6$ fermions in $L = 12$ sites. The initial state $|\psi^R(0)\rangle$ is the ground state for $\alpha = 0$ and is $(|101010101010\rangle + |010101010101\rangle)/\sqrt{2}$ for $\alpha = 1$ [133].

opens up. When we turn on the non-Hermiticity and nonreciprocity instead of the interaction, such that $\alpha = 1$ and $g = 0$ [Figs. 2(c1) and 2(c2)], $\rho(x)$ is oscillating around 0.5, and the spectrum becomes complex with L starlike spikes [133]. Note that it is not a superposition of the energies of N Hatano-Nelson chains [134–136], since Pauli exclusion constrains certain asymmetric hoppings.

Finally, turning on both the interaction and non-Hermiticity such that $\alpha = 1$ and $g = -100$ [Figs. 2(d1) and 2(d2)], we observe a peculiar state with an asymmetric profile $\rho(x)$ around the impurity at $x_0 + 1$, which we name a "squeezed polaron." The density to the left of $x_0 + 1 = 7$ (sites 5 and 6) appears to be "squeezed" towards the right (sites 8 and 9) by the impurity interaction, even though, naively, we would have expected the asymmetric $e^{\pm\alpha}\hat{c}_x\hat{c}_{x\pm1}$ couplings to pump the states from right to left instead. Notably, the $\rho(x)$ peak is not exponentially high like topological or non-Hermitian skin states, but instead resembles a finite local dipole within the Fermi sea. The spectrum is complex, and a gap separates two almost identical starlike "bands," the
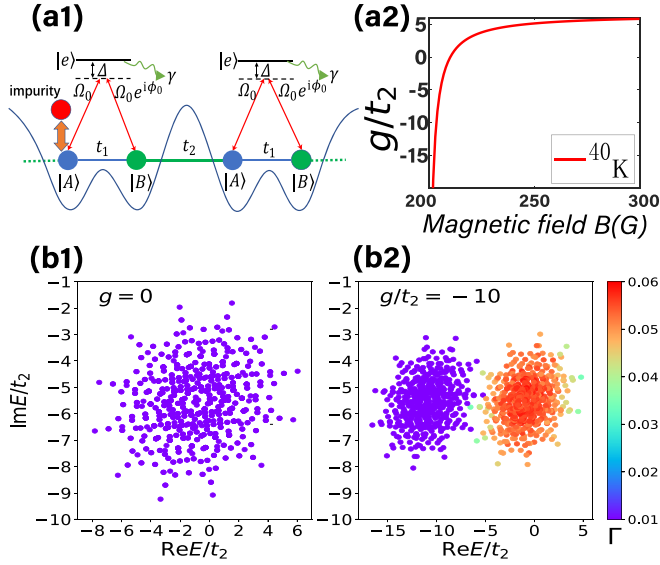
FIG. 3. (a1) Our effective interacting Hamiltonian for squeezed polarons [Eq. (5)] is based on a two-photon dissipative Raman process [29,74] with impurity interactions g from Feshbach resonance. The Rabi frequency is Ω_0 between hyperfine ground states $|A\rangle$ and $|B\rangle$ and the excited state $|e\rangle$ for ^{40}K atoms; a phase difference ϕ_0 introduces nonreciprocity. Δ is the single-photon detuning of the excited state $|e\rangle$, whose non-Hermitian decay rate γ can be laser controlled. (a2) The impurity interaction g is highly tunable through the magnetic field, with parameters given by Refs. [139–141]. (b1, b2) g nonperturbatively modifies the PBC spectrum E at half-filling $N = 6$ and $2L = 12$, such that all states $|\psi\rangle$ become squeezed with elevated squeezing asymmetry Γ when $|g| \neq 0$. Here, $t_2 = (2\pi) \times 1000$ Hz [142] sets the energy scale.

one with negative $\text{Re}(E)$ containing states bounded by the attractive ($g < 0$) impurity interaction.

Interestingly, even though the impurity interaction acts locally, its presence affects the *entire* spectrum [Fig. 2(d1)], not just states localized around the impurity. This is most saliently revealed through the squeezing asymmetry parameter Γ of a given N-fermion state $|\psi\rangle$, which we define as

$$\Gamma \equiv \sum_{x=1}^{L} (x - x_0 - 1) e^{-(x-x_0-1)^2} |\langle \psi | \hat{n}_x | \psi \rangle|^2 / N. \quad (3)$$

Containing the derivative of a Gaussian kernel, it measures the extent of asymmetric state localization around the the impurity neighbor $x_0 + 1$, unlike the more commonly used inverse participation ratio parameter [137], which is agnostic to the localization asymmetry and position. In particular, it distinguishes our squeezed polarons from ordinary polarons in Hermitian settings, which are symmetric about the impurity. As a reference, a profile with a perfectly localized surplus particle on each side has $\Gamma = 2/(Ne) \approx 0.74/N$, which is just slightly higher than the Γ of the eigenstates with polaron squeezing behavior [Figs. 2(d1) and 3(b2)]. This also implies that the squeezed polaron is distributed across *all* bound states, and not particular ground states as with ordinary polarons. Physically, this is because the impurity interaction has become effectively nonlocal in the background of nonreciprocal gain and loss pumping; but contrary to a

simple pumping of states, what we observe is an interaction-facilitated "squeezing" in the opposite direction that results in a dipolelike density profile. Herein lies an important physical distinction between Hermitian polarons and non-Hermitian squeezed polarons—while squeezed polaron asymmetry can be observed in the long-time steady state evolved from most generic initial states [138] [Fig. 2(e2)], Hermitian (symmetric) polaron localization only exists for the ground state (Fig. S8 of [133]).

Ultracold atomic model for observing squeezed polarons. Having discussed the essential though simplified mechanism behind squeezed polarons, we now turn to a more realistic setup without asymmetric physical couplings and that can be feasibly implemented in an ultracold atomic setup.

The key ingredients for squeezed polarons are (i) impurity interaction, (ii) nonreciprocity, and (iii) loss. To incorporate them all, we consider a one-dimensional fermionic array of N fermionic ^{40}K atoms, with the majority being spin $\uparrow$ and the minority being spin $\downarrow$ impurities.

To implement the impurity interaction (i), we apply an external magnetic field B that causes the atoms to experience a strong Feshbach resonance [140,141,143–149] that corresponds to a density-density S-wave interaction,

$$\hat{H}_{\text{int}} = g\hat{n}_{x_0,s}^{(b)} \hat{n}_{x_0,s}, \quad (4)$$

between unlike (majority and impurity) spins, where $\hat{n}_{x_0,s}^{(b)} = \hat{b}_{x_0,s}^{\dagger} \hat{b}_{x_0,s}$ is the number density operator of the spin-$\downarrow$ impurity atom, which is situated at site s of the x_0th unit cell, and $\hat{n}_{x_0,s} = \hat{c}_{x_0,s}^{\dagger} \hat{c}_{x_0,s}$ is the corresponding density operator of spin-$\uparrow$ majority atoms at the same position. The interaction strength $g \sim g_0(B - B_c)^{-1}$ becomes very strong and saturates at a large value near a resonant magnetic field [150] $B = B_c$, as numerically computed [141,143–146] and plotted in Fig. 3(a2), and can be tuned to any desired strength between $-1000t_2$ and $\approx 1500t_2$ by appropriately adjusting the field strength [133].

A nonreciprocal lattice with loss [(ii) and (iii)] can be achieved by coupling a two-photon dissipative Raman process to the discrete hyperfine ground states $|A\rangle$ and $|B\rangle$ [27,29,74,151–157] of each degenerate ^{40}K atom and subjecting the atoms to a strong periodic optical potential [29,142,158], as schematically illustrated in Fig. 3(a1). Nonreciprocity is introduced through the phase difference ϕ_0 between the optical fields exciting each hyperfine state; for maximum time-reversal breaking, we set $\phi_0 = \pi/2$. By adiabatically eliminating [133] the excited state $|e\rangle$, one obtains an effective spin-orbit coupling in the pseudospin basis of $|A\rangle$ and $|B\rangle$. If the excited state additionally experiences laser-induced decay of rate γ, the coupling becomes effectively complex [133], leading to an effective tight-binding Hamiltonian ($\hbar = 1$),

$$\hat{H} = \sum_{x}^{L} [(t_1 + \tilde{\gamma})\hat{c}_{x,A}^{\dagger}\hat{c}_{x,B} + (t_1 - \tilde{\gamma})\hat{c}_{x,B}^{\dagger}\hat{c}_{x,A}$$
$$+ t_2(\hat{c}_{x+1,A}^{\dagger}\hat{c}_{x,B} + \text{H.c.})] + g\hat{n}_{x_0,s}^{(b)}\hat{n}_{x_0,s} - i\tilde{\gamma}\sum_{x,s}^{L}\hat{n}_{x,s}, \quad (5)$$

where t_1 and t_2 depend on the optical potential [133] and

$$\tilde{\gamma} = \frac{\Omega_0^2}{\gamma + i\Delta} \tag{6}$$

is the effective decay rate, where Ω_0 and Δ are the single-photon Rabi frequency and detuning respectively. The effective intracell hoppings $t_1 \pm \tilde{\gamma}$ have become asymmetric and complex due to the combination of the reciprocity breaking and dissipation, even though the physical optical lattice couplings are all symmetric [133].

Before presenting the numerical results on this model, we briefly outline the experimental specifications for the parameters used. First, a tiny fraction of spin-↓ "impurity" atoms can be created by exciting a spin-polarized (spin-↑) cloud of ^{40}K atoms in the two lowest hyperfine states [87,90] via a two-photon Landau-Zener sweep and subsequently cooling it down. The resultant Fermi gas is then loaded onto a one-dimensional optical superlattice potential $V(x)$ [142,158], which is formed by superimposing two standing optical lasers with wavelengths $\lambda_2 = 767$ nm (short lattice) and $\lambda_1 = 2\lambda_2$ (long lattice) [142,158], such that $V(x) = V_1 \sin^2(k_1 x + \phi_0/2) + V_2 \sin^2(k_2 x + \pi/2)$, where $k_1 = 2\pi/\lambda_1$ and $k_2 = 2k_1$, corresponding to a unit cell of size $d = 767$ nm [142]. By adjusting the laser amplitudes V_1 and V_2, the effective lattice couplings t_1 and t_2 can be tuned within $(2\pi) \times [60, 1000]$ Hz [133,142]; in this work, we set $t_2 = (2\pi) \times 1000$ Hz [142] as the reference energy unit, and we fix $t_1/t_2 = 1$. For the two-photon dissipative Raman process, we use $\Omega_0 = (2\pi) \times 0.03$ MHz [159] and $\Delta = (2\pi) \times 1$ MHz for the single-photon Rabi frequency and detuning, and we fix the adjustable decay rate from the excited state $|e\rangle$ as $\gamma = (2\pi) \times 6$ MHz [159–161], such that the effective decay rate takes the value $\tilde{\gamma} \sim (0.92 - 0.15i)t_2 = (2\pi) \times (0.92 - 0.15i)$ kHz [133]. We fix the impurity at site $s = A$ of the x_0th cell. In all, lasers are employed for various distinct purposes: defining the optical lattice potential, sweeping to produce the impurities, and Raman transitions and laser-induced dissipation as shown in Fig. 3(a1).

As evident in Figs. 3(b1) and 3(b2), the effective ultracold-atomic Hamiltonian $\hat{H}$ of Eq. (5) captures the essential polaron behavior already present in the minimal single-component model $\hat{H}_{\min}$ of Eq. (1), with qualitatively similar many-body spectra. At a relatively modest interaction strength of $g = -10t_2$, corresponding to $B \approx 203.5$ G, the spectrum separates into two distinct "bands," both of which correspond to squeezed eigenstates. Their squeezed profile $\rho(x)$ (Figs. S6(a1)–S6(d1) [133]) also retains the characteristic asymmetrically squeezed shape, although it also exhibits step-like kinks due to the symmetry breaking from odd (even) $|A\rangle$ ($|B\rangle$) sites [133].

Attractive vs repulsive polaron squeezing. Figure 4(a) shows the squeezing expectation $|\Gamma|$ [162] in the parameter space of g/t_2, the normalized impurity interaction strength, and $|\tilde{\gamma}|/t_2$, the normalized effects of reciprocity and dissipation. For Hermitian scenarios with $|\tilde{\gamma}| = 0$ and $g \neq 0$, we indeed have vanishing Γ, as expected from ordinary polarons with symmetric impurity localizations. In general, the squeezing expectation $|\Gamma|$ increases with larger $|\tilde{\gamma}|$ or $|g|$, consistent with the intuition that polaron squeezing requires
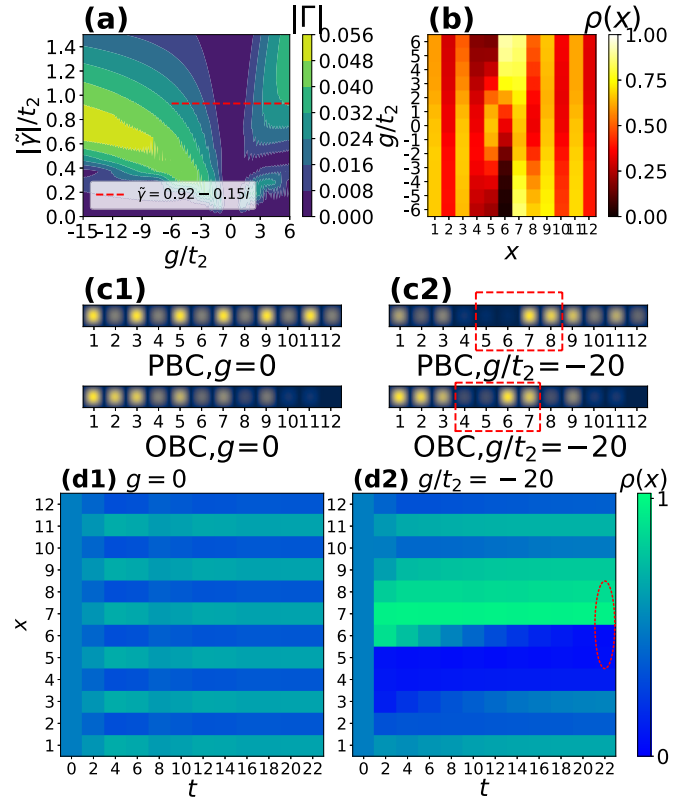

FIG. 4. (a) Squeezing expectation $|\Gamma|$ in the g-$|\tilde{\gamma}|$ parameter space; note the vanishing squeezing at zero impurity interaction g and the enhanced polaron squeezing at large effective decay rate $|\tilde{\gamma}|$ and very attractive ($g < 0$) or repulsive ($g > 0$) interactions. Here, Γ is computed from the long-time steady state evolved from the initial state $|\psi^R(0)\rangle = (|101010101010\rangle + |010101010101\rangle)/\sqrt{2}$. (b) Spatial density $\rho(x)$ as a function of x and g under PBCs. Note the very pronounced asymmetric profile across the impurity position $x_0 = 6$, particularly in the repulsive ($g > 0$) case where $\rho(x_0)$ is strongly localized. Data are plotted at $\tilde{\gamma}/t_2 = 0.92 - 0.15i$, as indicated by the dashed red line in panel (a). (c1, c2) Simulated spatial density measurements. The density around the impurity ($x_0 + 1 = 7$) exhibits almost identical asymmetric profiles of squeezed polaron states (red dashed box) regardless of OBCs or PBCs, as long as the impurity interaction g is nonzero, with a slight shift from sublattice effects. (d1, d2) Evolution of spatial densities from the initial state $|\psi^R(0)\rangle$ under PBCs, with an asymmetric steady-state squeezed polaron profile for (d2) $g \neq 0$. We used $\tilde{\gamma}/t_2 = 0.92 - 0.15i$, $t_1/t_2 = 1$, and $N = 6$ fermions in $2L = 12$ sites for all subfigures, and we used $g = 0$ for panels (c1) and (d1) and $g/t_2 = -20$ for panels (c2) and (d2).

the combined interplay of interactions, nonreciprocity and non-Hermiticity.

However, Fig. 4(a) also shows a marked asymmetry between attractive ($g < 0$) and repulsive ($g > 0$) squeezed polarons. A stronger interaction is required to produce an attractive squeezed polaron, relative to a comparably squeezed repulsive polaron. The reason behind this is clear from the plot of spatial density $\rho(x)$ vs g/t_2 [see Fig. 4(b)], evaluated at the value of $\tilde{\gamma}_2 = 0.92 - 0.15i$ used in Fig. 3. For attractive polarons with $g < 0$, $\rho(x)$ is strongly localized at $x_0 + 1 = 7$

next to the impurity, leaving a "hole" at the impurity. However, for repulsive polarons with $g > 0$, $\rho(x)$ is strongly localized at the impurity position $x_0 = 6$. That said, for both attractive and repulsive cases, the asymmetry in the $\rho(x)$ profile is still strongly contributed by the $\tilde{\gamma}$ asymmetry. In all, repulsive polarons generally possess a stronger combined "dipole" moment and hence larger Γ.

Independence from boundary conditions. While we have emphasized that squeezed polarons, unlike skin or topological states, are interacting phenomena and not boundary phenomena, actual experimental lattices are usually bounded [163]. Fortunately, that is not a practical obstacle, because squeezed polarons are largely unaffected by boundary conditions, be they OBCs or PBCs. Shown in Fig. 4(c), there are simulated spatial density of states for $\rho(x)$ measurements with $N = 6$ fermions on $2L = 12$ sites and the impurity at $x_0 = 6$. Without interactions, i.e., $g = 0$ (left), we observe skin boundary accumulation under OBCs but not PBCs. However, squeezed polaron physics dominates in the bulk when the impurity interaction is turned on (right). For both PBCs and OBCs, approximately equal Fermi polaron squeezing (red highlighted) counteracts the background skin accumulation, if any. Despite finite-size effects, polaron squeezing is evidently a robust non-Hermitian interaction effect distinguishable from competing single-body effects away from the boundaries.

Discussion. With very recent breakthroughs in non-Hermitian cold-atom experiments [24–29], the physical realization of interacting many-body effects is closer to becoming a practical reality even in non-Hermitian settings. We are hopeful that, through our proposal, squeezed polarons can be measured in the near future, thereby realizing a many-body form of emergent nonlocality distinct from non-Hermitian skin sensitivity.

While a squeezed polaron manifests as a local dipolelike density asymmetry, not colossal exponential state localization, it nonperturbatively splits the *entire* spectrum into two halves, a fascinating demonstration of how particle statistics can help encode nonlocal effects despite seemingly local density effects. While we have largely demonstrated polaron squeezing with PBCs, it occurs independently of boundaries and remains robust in realistic experimental setups subject to OBCs.

[1] L. Feng, M. Ayache, J. Huang, Y.-L. Xu, M.-H. Lu, Y.-F. Chen, Y. Fainman, and A. Scherer, Nonreciprocal light propagation in a silicon photonic circuit, Science **333**, 729 (2011).

[2] Z. Shen, Y.-L. Zhang, Y. Chen, C.-L. Zou, Y.-F. Xiao, X.-B. Zou, F.-W. Sun, G.-C. Guo, and C.-H. Dong, Experimental realization of optomechanically induced non-reciprocity, Nat. Photonics **10**, 657 (2016).

[3] S. H. Park, S.-G. Lee, S. Baek, T. Ha, S. Lee, B. Min, S. Zhang, M. Lawrence, and T.-T. Kim, Observation of an exceptional point in a non-Hermitian metasurface, Nanophotonics **9**, 1031 (2020).

[4] C. Coulais, D. Sounas, and A. Alù, Static non-reciprocity in mechanical metamaterials, Nature (London) **542**, 461 (2017).

[5] W. Zhu, X. Fang, D. Li, Y. Sun, Y. Li, Y. Jing, and H. Chen, Simultaneous Observation of a Topological Edge State and Exceptional Point in an Open and Non-Hermitian Acoustic System, Phys. Rev. Lett. **121**, 124501 (2018).

[6] A. Ghatak, M. Brandenbourger, J. van Wezel, and C. Coulais, Observation of non-Hermitian topology and its bulk–edge correspondence in an active mechanical metamaterial, Proc. Natl. Acad. Sci. U.S.A. **117**, 29561 (2020).

[7] M. Brandenbourger, X. Locsin, E. Lerner, and C. Coulais, Non-reciprocal robotic metamaterials, Nat. Commun. **10**, 4608 (2019).

[8] H. Gao, H. Xue, Z. Gu, T. Liu, J. Zhu, and B. Zhang, Non-Hermitian route to higher-order topology in an acoustic crystal, Nat. Commun. **12**, 1888 (2021).

[9] T. Helbig, T. Hofmann, S. Imhof, M. Abdelghany, T. Kiessling, L. Molenkamp, C. Lee, A. Szameit, M. Greiter, and R. Thomale, Generalized bulk–boundary correspondence in non-Hermitian topolectrical circuits, Nat. Phys. **16**, 747 (2020).

[10] T. Hofmann, T. Helbig, C. H. Lee, M. Greiter, and R. Thomale, Chiral Voltage Propagation and Calibration in a Topolectrical Chern Circuit, Phys. Rev. Lett. **122**, 247702 (2019).

[11] S. Liu, S. Ma, C. Yang, L. Zhang, W. Gao, Y. J. Xiang, T. J. Cui, and S. Zhang, Gain- and Loss-Induced Topological Insulating Phase in a Non-Hermitian Electrical Circuit, Phys. Rev. Appl. **13**, 014047 (2020).

[12] T. Hofmann, T. Helbig, F. Schindler, N. Salgo, M. Brzezińska, M. Greiter, T. Kiessling, D. Wolf, A. Vollhardt, A. Kabaši *et al.*, Reciprocal skin effect and its realization in a topolectrical circuit, Phys. Rev. Res. **2**, 023265 (2020).

[13] S. Liu, R. Shao, S. Ma, L. Zhang, O. You, H. Wu, Y. J. Xiang, T. J. Cui, and S. Zhang, Non-Hermitian skin effect in a non-Hermitian electrical circuit, Research **2021**, 5608038 (2021).

[14] D. Zou, T. Chen, W. He, J. Bao, C. H. Lee, H. Sun, and X. Zhang, Observation of hybrid higher-order skin-topological effect in non-Hermitian topolectrical circuits, Nat. Commun. **12**, 7201 (2021).

[15] A. Stegmaier, S. Imhof, T. Helbig, T. Hofmann, C. H. Lee, M. Kremer, A. Fritzsche, T. Feichtner, S. Klembt, S. Höfling *et al.*, Topological Defect Engineering and $\mathcal{PT}$ symmetry in Non-Hermitian Electrical Circuits, Phys. Rev. Lett. **126**, 215302 (2021).

[16] C. Shang, S. Liu, R. Shao, P. Han, X. Zang, X. Zhang, K. N. Salama, W. Gao, C. H. Lee, R. Thomale, A. Manchon, S. Zhang, T. J. Cui, and U. Schwingenschlögl, Experimental identification of the second-order non-Hermitian skin

effect with physics-graph-informed machine learning, Adv. Sci. **9**, 2202922 (2022).

[17] L. Xiao, T. Deng, K. Wang, G. Zhu, Z. Wang, W. Yi, and P. Xue, Non-Hermitian bulk–boundary correspondence in quantum dynamics, Nat. Phys. **16**, 761 (2020).

[18] L. Feng, R. El-Ganainy, and L. Ge, Non-Hermitian photonics based on parity–time symmetry, Nat. Photonics **11**, 752 (2017).

[19] L. D. Tzuang, K. Fang, P. Nussenzveig, S. Fan, and M. Lipson, Non-reciprocal phase shift induced by an effective magnetic flux for light, Nat. Photonics **8**, 701 (2014).

[20] H. Zhou, C. Peng, Y. Yoon, C. W. Hsu, K. A. Nelson, L. Fu, J. D. Joannopoulos, M. Soljačić, and B. Zhen, Observation of bulk Fermi arc and polarization half charge from paired exceptional points, Science **359**, 1009 (2018).

[21] B. Zhen, C. W. Hsu, Y. Igarashi, L. Lu, I. Kaminer, A. Pick, S.-L. Chua, J. D. Joannopoulos, and M. Soljačić, Spawning rings of exceptional points out of Dirac cones, Nature (London) **525**, 354 (2015).

[22] J. M. Zeuner, M. C. Rechtsman, Y. Plotnik, Y. Lumer, S. Nolte, M. S. Rudner, M. Segev, and A. Szameit, Observation of a Topological Transition in the Bulk of a Non-Hermitian System, Phys. Rev. Lett. **115**, 040402 (2015).

[23] M.-A. Miri and A. Alù, Exceptional points in optics and photonics, Science **363**, eaar7709 (2019).

[24] J. Li, A. K. Harter, J. Liu, L. de Melo, Y. N. Joglekar, and L. Luo, Observation of parity-time symmetry breaking transitions in a dissipative Floquet system of ultracold atoms, Nat. Commun. **10**, 855 (2019).

[25] S. Lapp, F. A. An, B. Gadway *et al.*, Engineering tunable local loss in a synthetic lattice of momentum states, New J. Phys. **21**, 045006 (2019).

[26] Z. Ren, D. Liu, E. Zhao, C. He, K. K. Pak, J. Li, and G.-B. Jo, Chiral control of quantum states in non-Hermitian spin–orbit-coupled fermions, Nat. Phys. **18**, 385 (2022).

[27] Q. Liang, D. Xie, Z. Dong, H. Li, H. Li, B. Gadway, W. Yi, and B. Yan, Dynamic Signatures of Non-Hermitian Skin Effect and Topology in Ultracold Atoms, Phys. Rev. Lett. **129**, 070401 (2022).

[28] W. Yi, An exceptional mass dance, Nat. Phys. **18**, 370 (2022).

[29] W. Gou, T. Chen, D. Xie, T. Xiao, T.-S. Deng, B. Gadway, W. Yi, and B. Yan, Tunable Nonreciprocal Quantum Transport through a Dissipative Aharonov-Bohm Ring in Ultracold Atoms, Phys. Rev. Lett. **124**, 070402 (2020).

[30] E. J. Bergholtz, J. C. Budich, and F. K. Kunst, Exceptional topology of non-Hermitian systems, Rev. Mod. Phys. **93**, 015005 (2021).

[31] E. Lafalce, Q. Zeng, C. H. Lin, M. J. Smith, S. T. Malak, J. Jung, Y. J. Yoon, Z. Lin, V. V. Tsukruk, and Z. V. Vardeny, Robust lasing modes in coupled colloidal quantum dot microdisk pairs using a non-Hermitian exceptional point, Nat. Commun. **10**, 561 (2019).

[32] V. Kozii and L. Fu, Non-Hermitian topological theory of finite-lifetime quasiparticles: Prediction of bulk Fermi arc due to exceptional point, arXiv:1708.05841.

[33] T. Yoshida and Y. Hatsugai, Exceptional rings protected by emergent symmetry for mechanical systems, Phys. Rev. B **100**, 054109 (2019).

[34] T. Yoshida, R. Peters, N. Kawakami, and Y. Hatsugai, Symmetry-protected exceptional rings in two-dimensional

correlated systems with chiral symmetry, Phys. Rev. B **99**, 121101(R) (2019).

[35] R. Okugawa and T. Yokoyama, Topological exceptional surfaces in non-Hermitian systems with parity-time and parity-particle-hole symmetries, Phys. Rev. B **99**, 041202(R) (2019).

[36] H. Hodaei, A. U. Hassan, S. Wittek, H. Garcia-Gracia, R. El-Ganainy, D. N. Christodoulides, and M. Khajavikhan, Enhanced sensitivity at higher-order exceptional points, Nature (London) **548**, 187 (2017).

[37] D. Heiss, Circling exceptional points, Nat. Phys. **12**, 823 (2016).

[38] W. Heiss, The physics of exceptional points, J. Phys. A: Math. Theor. **45**, 444016 (2012).

[39] Z. Gong, Y. Ashida, K. Kawabata, K. Takasan, S. Higashikawa, and M. Ueda, Topological Phases of Non-Hermitian Systems, Phys. Rev. X **8**, 031079 (2018).

[40] T. Yoshida, R. Peters, and N. Kawakami, Non-Hermitian perspective of the band structure in heavy-fermion systems, Phys. Rev. B **98**, 035141 (2018).

[41] K. Zhang, Z. Yang, and C. Fang, Correspondence between Winding Numbers and Skin Modes in Non-Hermitian Systems, Phys. Rev. Lett. **125**, 126402 (2020).

[42] Q. Zhong, M. Khajavikhan, D. N. Christodoulides, and R. El-Ganainy, Winding around non-Hermitian singularities, Nat. Commun. **9**, 1 (2018).

[43] S. M. Rafi-Ul-Islam, Z. B. Siu, and M. B. A. Jalil, Topological phases with higher winding numbers in nonreciprocal one-dimensional topolectrical circuits, Phys. Rev. B **103**, 035420 (2021).

[44] T. Yoshida, T. Mizoguchi, and Y. Hatsugai, Mirror skin effect and its electric circuit simulation, Phys. Rev. Res. **2**, 022062(R) (2020).

[45] G. Sun, J.-C. Tang, and S.-P. Kou, Biorthogonal quantum criticality in non-Hermitian many-body systems, Front. Phys. **17**, 33502 (2022).

[46] W. Xi, Z.-H. Zhang, Z.-C. Gu, and W.-Q. Chen, Classification of topological phases in one dimensional interacting non-Hermitian systems and emergent unitarity, Sci. Bull. **66**, 1731 (2021).

[47] C. H. Lee, L. Li, R. Thomale, and J. Gong, Unraveling non-Hermitian pumping: Emergent spectral singularities and anomalous responses, Phys. Rev. B **102**, 085151 (2020).

[48] L. Li and C. H. Lee, Non-Hermitian pseudo-gaps, Sci. Bull. **67**, 685 (2022).

[49] L. Li, C. H. Lee, S. Mu, and J. Gong, Critical non-Hermitian skin effect, Nat. Commun. **11**, 1 (2020).

[50] P.-Y. Chang, J.-S. You, X. Wen, and S. Ryu, Entanglement spectrum and entropy in topological non-Hermitian systems and nonunitary conformal field theory, Phys. Rev. Res. **2**, 033069 (2020).

[51] C. H. Lee, Exceptional Bound States and Negative Entanglement Entropy, Phys. Rev. Lett. **128**, 010402 (2022).

[52] N. Okuma and M. Sato, Quantum anomaly, non-Hermitian skin effects, and entanglement entropy in open systems, Phys. Rev. B **103**, 085428 (2021).

[53] S. Yao and Z. Wang, Edge States and Topological Invariants of Non-Hermitian Systems, Phys. Rev. Lett. **121**, 086803 (2018).

[54] Y. Xiong, Why does bulk boundary correspondence fail in some non-Hermitian topological models, J. Phys. Commun. **2**, 035043 (2018).

[55] C. H. Lee and R. Thomale, Anatomy of skin modes and topology in non-Hermitian systems, Phys. Rev. B **99**, 201103(R) (2019).

[56] F. K. Kunst, E. Edvardsson, J. C. Budich, and E. J. Bergholtz, Biorthogonal Bulk-Boundary Correspondence in Non-Hermitian Systems, Phys. Rev. Lett. **121**, 026808 (2018).

[57] K. Yokomizo and S. Murakami, Non-Bloch Band Theory of Non-Hermitian Systems, Phys. Rev. Lett. **123**, 066404 (2019).

[58] K.-I. Imura and Y. Takane, Generalized bulk-edge correspondence for non-Hermitian topological systems, Phys. Rev. B **100**, 165430 (2019).

[59] L. Jin and Z. Song, Bulk-boundary correspondence in a non-Hermitian system in one dimension with chiral inversion symmetry, Phys. Rev. B **99**, 081103(R) (2019).

[60] D. S. Borgnia, A. J. Kruchkov, and R.-J. Slager, Non-Hermitian Boundary Modes and Topology, Phys. Rev. Lett. **124**, 056802 (2020).

[61] L. Li, S. Mu, C. H. Lee, and J. Gong, Quantized classical response from spectral winding topology, Nat. Commun. **12**, 5294 (2021).

[62] C. Lv, R. Zhang, Z. Zhai, and Q. Zhou, Curving the space by non-Hermiticity, Nat. Commun. **13**, 2184 (2022).

[63] R. Yang, J. W. Tan, T. Tai, J. M. Koh, L. Li, S. Longhi, and C. H. Lee, Designing non-Hermitian real spectra through electrostatics, Sci. Bull. **67**, 1865 (2022).

[64] H. Jiang and C. H. Lee, Dimensional transmutation from non-Hermiticity, arXiv:2207.08843.

[65] T. Tai and C. H. Lee, Zoology of non-Hermitian spectra and their graph topology, arXiv:2202.03462.

[66] R. Hamazaki, K. Kawabata, and M. Ueda, Non-Hermitian Many-Body Localization, Phys. Rev. Lett. **123**, 090603 (2019).

[67] L.-J. Zhai, S. Yin, and G.-Y. Huang, Many-body localization in a non-Hermitian quasiperiodic system, Phys. Rev. B **102**, 064206 (2020).

[68] K. Suthar, Y.-C. Wang, Y.-P. Huang, H. H. Jen, and J.-S. You, Non-Hermitian many-body localization with open boundaries, Phys. Rev. B **106**, 064208 (2022).

[69] Y.-C. Wang, K. Suthar, H. Jen, Y.-T. Hsu, and J.-S. You, Non-Hermitian skin effects on many-body localized and thermal phases, arXiv:2210.12998.

[70] M. Luo, Skin effect and excitation spectral of interacting non-Hermitian system, arXiv:2001.00697.

[71] D.-W. Zhang, Y.-L. Chen, G.-Q. Zhang, L.-J. Lang, Z. Li, and S.-L. Zhu, Skin superfluid, topological Mott insulators, and asymmetric dynamics in an interacting non-Hermitian Aubry-André-Harper model, Phys. Rev. B **101**, 235150 (2020).

[72] T. Liu, J. J. He, T. Yoshida, Z.-L. Xiang, and F. Nori, Non-Hermitian topological Mott insulators in one-dimensional fermionic superlattices, Phys. Rev. B **102**, 235151 (2020).

[73] L. Zhou and X. Cui, Enhanced fermion pairing and superfluidity by an imaginary magnetic field, iScience **14**, 257 (2019).

[74] L. Zhou, W. Yi, and X. Cui, Dissipation-facilitated molecules in a Fermi gas with non-Hermitian spin-orbit coupling, Phys. Rev. A **102**, 043310 (2020).

[75] J.-S. Pan, W. Yi, and J. Gong, Emergent pt-symmetry breaking of collective modes with topological critical phenomena, Commun. Phys. **4**, 261 (2021).

[76] C. H. Lee, Many-body topological and skin states without open boundaries, Phys. Rev. B **104**, 195102 (2021).

[77] R. Shen and C. H. Lee, Non-Hermitian skin clusters from strong interactions, Commun. Phys. **5**, 238 (2022).

[78] L. Pan, X. Chen, Y. Chen, and H. Zhai, Non-Hermitian linear response theory, Nat. Phys. **16**, 767 (2020).

[79] K. Kawabata, K. Shiozaki, and S. Ryu, Many-body topology of non-Hermitian systems, Phys. Rev. B **105**, 165137 (2022).

[80] K. Yamamoto, M. Nakagawa, K. Adachi, K. Takasan, M. Ueda, and N. Kawakami, Theory of Non-Hermitian Fermionic Superfluidity with a Complex-Valued Interaction, Phys. Rev. Lett. **123**, 123601 (2019).

[81] F. Alsallom, L. Herviou, O. V. Yazyev, and M. Brzezińska, Fate of the non-Hermitian skin effect in many-body fermionic systems, Phys. Rev. Res. **4**, 033122 (2022).

[82] S.-B. Zhang, M. M. Denner, T. Bzdušek, M. A. Sentef, and T. Neupert, Symmetry breaking and spectral structure of the interacting Hatano-Nelson model, Phys. Rev. B **106**, L121102 (2022).

[83] A. N. Poddubny, Topologically bound states, non-Hermitian skin effect and flat bands, induced by two-particle interaction, arXiv:2211.06043.

[84] T. Yoshida and Y. Hatsugai, Fate of exceptional points under interactions: Reduction of topological classifications, arXiv:2211.08895.

[85] P. Weinberg and M. Bukov, QuSpin: A Python package for dynamics and exact diagonalisation of quantum many body systems. Part I: spin chains, SciPost Phys. **2**, 003 (2017).

[86] P. Weinberg and M. Bukov, Quspin: A Python package for dynamics and exact diagonalisation of quantum many body systems. Part II: Bosons, fermions and higher spins, SciPost Phys. **7**, 020 (2019).

[87] A. Schirotzek, C.-H. Wu, A. Sommer, and M. W. Zwierlein, Observation of Fermi Polarons in a Tunable Fermi Liquid of Ultracold Atoms, Phys. Rev. Lett. **102**, 230402 (2009).

[88] Y. Zhang, W. Ong, I. Arakelyan, and J. E. Thomas, Polaron-to-Polaron Transitions in the Radio-Frequency Spectrum of a Quasi-Two-Dimensional Fermi Gas, Phys. Rev. Lett. **108**, 235302 (2012).

[89] C. Kohstall, M. Zaccanti, M. Jag, A. Trenkwalder, P. Massignan, G. M. Bruun, F. Schreck, and R. Grimm, Metastability and coherence of repulsive polarons in a strongly interacting Fermi mixture, Nature (London) **485**, 615 (2012).

[90] M. Koschorreck, D. Pertot, E. Vogt, B. Frohlich, M. Feld, and M. Kohl, Attractive and repulsive Fermi polarons in two dimensions, Nature (London) **485**, 619 (2012).

[91] M. Cetina, M. Jag, R. S. Lous, I. Fritsche, J. T. M. Walraven, R. Grimm, J. Levinsen, M. M. Parish, R. Schmidt, M. Knap *et al.*, Ultrafast many-body interferometry of impurities coupled to a Fermi sea, Science **354**, 96 (2016).

[92] F. Scazza, G. Valtolina, P. Massignan, A. Recati, A. Amico, A. Burchianti, C. Fort, M. Inguscio, M. Zaccanti, and G. Roati, Repulsive Fermi Polarons in a Resonant Mixture of Ultracold ^{6}Li Atoms, Phys. Rev. Lett. **118**, 083602 (2017).

[93] Z. Yan, P. B. Patel, B. Mukherjee, R. J. Fletcher, J. Struck, and M. W. Zwierlein, Boiling a Unitary Fermi Liquid, Phys. Rev. Lett. **122**, 093401 (2019).

[94] N. Darkwah Oppong, L. Riegger, O. Bettermann, M. Höfer, J. Levinsen, M. M. Parish, I. Bloch, and S. Fölling, Observation of Coherent Multiorbital Polarons in a Two-Dimensional Fermi Gas, Phys. Rev. Lett. **122**, 193604 (2019).

[95] G. Ness, C. Shkedrov, Y. Florshaim, O. K. Diessel, J. von Milczewski, R. Schmidt, and Y. Sagi, Observation of a Smooth Polaron-Molecule Transition in a Degenerate Fermi Gas, Phys. Rev. X **10**, 041019 (2020).

[96] M.-G. Hu, M. J. Van de Graaff, D. Kedar, J. P. Corson, E. A. Cornell, and D. S. Jin, Bose Polarons in the Strongly Interacting Regime, Phys. Rev. Lett. **117**, 055301 (2016).

[97] N. B. Jørgensen, L. Wacker, K. T. Skalmstang, M. M. Parish, J. Levinsen, R. S. Christensen, G. M. Bruun, and J. J. Arlt, Observation of Attractive and Repulsive Polarons in a Bose-Einstein Condensate, Phys. Rev. Lett. **117**, 055302 (2016).

[98] Z. Z. Yan, Y. Ni, C. Robens, and M. W. Zwierlein, Bose polarons near quantum criticality, Science **368**, 190 (2020).

[99] H. Hu, L. Jiang, H. Pu, Y. Chen, and X.-J. Liu, Universal Impurity-Induced Bound State in Topological Superfluids, Phys. Rev. Lett. **110**, 020401 (2013).

[100] C. H. Lee and X.-L. Qi, Lattice construction of pseudopotential Hamiltonians for fractional chern insulators, Phys. Rev. B **90**, 085103 (2014).

[101] C. H. Lee, Z. Papić, and R. Thomale, Geometric Construction of Quantum Hall Clustering Hamiltonians, Phys. Rev. X **5**, 041003 (2015).

[102] F. Grusdt, N. Y. Yao, D. Abanin, M. Fleischhauer, and E. Demler, Interferometric measurements of many-body topological invariants using mobile impurities, Nat. Commun. **7**, 11994 (2016).

[103] A. Camacho-Guardian, N. Goldman, P. Massignan, and G. M. Bruun, Dropping an impurity into a chern insulator: A polaron view on topological matter, Phys. Rev. B **99**, 081105(R) (2019).

[104] D. Pimenov, A. Camacho-Guardian, N. Goldman, P. Massignan, G. M. Bruun, and M. Goldstein, Topological transport of mobile impurities, Phys. Rev. B **103**, 245106 (2021).

[105] F. Qin, X. Cui, and W. Yi, Polaron in a $p + ip$ Fermi topological superfluid, Phys. Rev. A **99**, 033613 (2019).

[106] F. Chevy, Universal phase diagram of a strongly interacting Fermi gas with unbalanced spin populations, Phys. Rev. A **74**, 063628 (2006).

[107] C. Lobo, A. Recati, S. Giorgini, and S. Stringari, Normal State of a Polarized Fermi Gas at Unitarity, Phys. Rev. Lett. **97**, 200403 (2006).

[108] R. Combescot, A. Recati, C. Lobo, and F. Chevy, Normal State of Highly Polarized Fermi Gases: Simple Many-Body Approaches, Phys. Rev. Lett. **98**, 180402 (2007).

[109] G. M. Bruun and P. Massignan, Decay of Polarons and Molecules in a Strongly Polarized Fermi Gas, Phys. Rev. Lett. **105**, 020403 (2010).

[110] C. J. M. Mathy, M. M. Parish, and D. A. Huse, Trimers, Molecules, and Polarons in Mass-Imbalanced Atomic Fermi Gases, Phys. Rev. Lett. **106**, 166404 (2011).

[111] S. Zöllner, G. M. Bruun, and C. Pethick, Polarons and molecules in a two-dimensional Fermi gas, Phys. Rev. A **83**, 021603(R) (2011).

[112] M. M. Parish, Polaron-molecule transitions in a two-dimensional Fermi gas, Phys. Rev. A **83**, 051603(R) (2011).

[113] J. Levinsen, P. Massignan, F. Chevy, and C. Lobo, *p*-Wave Polaron, Phys. Rev. Lett. **109**, 075302 (2012).

[114] W. Yi and W. Zhang, Molecule and Polaron in a Highly Polarized Two-Dimensional Fermi Gas with Spin-Orbit Coupling, Phys. Rev. Lett. **109**, 140402 (2012).

[115] M. M. Parish and J. Levinsen, Highly polarized Fermi gases in two dimensions, Phys. Rev. A **87**, 033616 (2013).

[116] W. Yi and X. Cui, Polarons in ultracold Fermi superfluids, Phys. Rev. A **92**, 013620 (2015).

[117] Y. Nishida, Polaronic Atom-Trimer Continuity in Three-Component Fermi Gases, Phys. Rev. Lett. **114**, 115302 (2015).

[118] M. M. Parish and J. Levinsen, Quantum dynamics of impurities coupled to a Fermi sea, Phys. Rev. B **94**, 184303 (2016).

[119] A. Camacho-Guardian, L. A. Pena Ardila, T. Pohl, and G. M. Bruun, Bipolarons in a Bose-Einstein Condensate, Phys. Rev. Lett. **121**, 013401 (2018).

[120] X. Cui, Fermi polaron revisited: Polaron-molecule transition and coexistence, Phys. Rev. A **102**, 061301(R) (2020).

[121] R. Pessoa, S. A. Vitiello, and L. A. Peña Ardila, Finite-range effects in the unitary Fermi polaron, Phys. Rev. A **104**, 043313 (2021).

[122] L. A. Peña Ardila, Dynamical formation of polarons in a Bose-Einstein condensate: A variational approach, Phys. Rev. A **103**, 033323 (2021).

[123] K. Seetharam, Y. Shchadilova, F. Grusdt, M. B. Zvonarev, and E. Demler, Dynamical Quantum Cherenkov Transition of Fast Impurities in Quantum Liquids, Phys. Rev. Lett. **127**, 185302 (2021).

[124] K. Seetharam, Y. Shchadilova, F. Grusdt, M. Zvonarev, and E. Demler, Quantum Cherenkov transition of finite momentum Bose polarons, arXiv:2109.12260.

[125] H. Hu, J. Wang, J. Zhou, and X.-J. Liu, Crossover polarons in a strongly interacting Fermi superfluid, Phys. Rev. A **105**, 023317 (2022).

[126] F. Qin, C. H. Lee, R. Chen *et al.*, Light-induced phase crossovers in a quantum spin Hall system, Phys. Rev. B **106**, 235405 (2022).

[127] F. Qin, R. Chen, and H.-Z. Lu, Phase transitions in intrinsic magnetic topological insulator with high-frequency pumping, J. Phys.: Condens. Matter **34**, 225001 (2022).

[128] F. Qin, S. Li, Z. Z. Du, C. M. Wang, W. Zhang, D. Yu, H.-Z. Lu, and X. C. Xie, Theory for the Charge-Density-Wave Mechanism of 3D Quantum Hall Effect, Phys. Rev. Lett. **125**, 206601 (2020).

[129] L. Li, C. H. Lee, and J. Gong, Impurity induced scale-free localization, Commun. Phys. **4**, 1 (2021).

[130] M. Z. Hasan and C. L. Kane, Colloquium: Topological insulators, Rev. Mod. Phys. **82**, 3045 (2010).

[131] C.-K. Chiu, J. C. Y. Teo, A. P. Schnyder, and S. Ryu, Classification of topological quantum matter with symmetries, Rev. Mod. Phys. **88**, 035005 (2016).

[132] For a more practical implementation involving physical flux, see the more realistic cold-atom Hamiltonian presented later.

[133] See Supplemental Material at http://link.aps.org/supplemental/10.1103/PhysRevA.107.L010202 for Section H "Non-Hermitian interaction model"; for adiabatically elimination, which includes Ref. [164–169]; for the derivation of the effective model, which includes Ref. [74,170–173]; and for mapping to tight-binding model, which includes Refs. [174–176].

[134] N. Hatano and D. R. Nelson, Localization Transitions in Non-Hermitian Quantum Mechanics, Phys. Rev. Lett. **77**, 570 (1996).

[135] N. Hatano and D. R. Nelson, Vortex pinning and non-Hermitian quantum mechanics, Phys. Rev. B **56**, 8651 (1997).

[136] N. Hatano and D. R. Nelson, Non-Hermitian delocalization and eigenfunctions, Phys. Rev. B **58**, 8384 (1998).

[137] S. Hikami, Localization length and inverse participation ratio of two dimensional electron in the quantized Hall effect, Prog. Theor. Phys. **76**, 1210 (1986).

[138] This is because a randomly given initial state would most likely overlap with some of the many eigenstates in the right (reddish) cluster of Fig. 2(d1).

[139] Y.-A. Liao, A. S. C. Rittner, T. Paprotta, W. Li, G. B. Partridge, R. G. Hulet, S. K. Baur, and E. J. Mueller, Spin-imbalance in a one-dimensional Fermi gas, Nature (London) **467**, 567 (2010).

[140] C. A. Regal, M. Greiner, and D. S. Jin, Observation of Resonance Condensation of Fermionic Atom Pairs, Phys. Rev. Lett. **92**, 040403 (2004).

[141] C. Chin, R. Grimm, P. Julienne, and E. Tiesinga, Feshbach resonances in ultracold gases, Rev. Mod. Phys. **82**, 1225 (2010).

[142] M. Atala, M. Aidelsburger, J. T. Barreiro, D. Abanin, T. Kitagawa, E. Demler, and I. Bloch, Direct measurement of the Zak phase in topological Bloch bands, Nat. Phys. **9**, 795 (2013).

[143] M. Olshanii, Atomic Scattering in the Presence of an External Confinement and a Gas of Impenetrable Bosons, Phys. Rev. Lett. **81**, 938 (1998).

[144] T. Bergeman, M. G. Moore, and M. Olshanii, Atom-Atom Scattering under Cylindrical Harmonic Confinement: Numerical and Analytic Studies of the Confinement Induced Resonance, Phys. Rev. Lett. **91**, 163201 (2003).

[145] F. Qin, P. Zhang, and P.-L. Zhao, Large-momentum tail of one-dimensional Fermi gases with spin-orbit coupling, Phys. Rev. A **101**, 063619 (2020).

[146] F. Qin and P. Zhang, Universal relations for hybridized *s*- and *p*-wave interactions from spin-orbital coupling, Phys. Rev. A **102**, 043321 (2020).

[147] C. A. Regal, C. Ticknor, J. L. Bohn, and D. S. Jin, Tuning *p*-Wave Interactions in an Ultracold Fermi Gas of Atoms, Phys. Rev. Lett. **90**, 053201 (2003).

[148] F. Qin, X. Cui, and W. Yi, Universal relations and normal phase of an ultracold Fermi gas with coexisting *s*- and *p*-wave interactions, Phys. Rev. A **94**, 063616 (2016).

[149] F. Qin, J.-S. Pan, S. Wang, and G.-C. Guo, Width of the confinement-induced resonance in a quasi-one-dimensional trap with transverse anisotropy, Eur. Phys. J. D **71**, 304 (2017).

[150] In practice, at very strong resonance, the scattering length diverges and a quantum halo state is formed instead.

[151] Y.-J. Lin, R. L. Compton, A. R. Perry, W. D. Phillips, J. V. Porto, and I. B. Spielman, Bose-Einstein Condensate in a Uniform Light-Induced Vector Potential, Phys. Rev. Lett. **102**, 130401 (2009).

[152] Y.-J. Lin, K. Jimenez-Garcia, and I. B. Spielman, Spin-orbit-coupled Bose-Einstein condensates, Nature (London) **471**, 83 (2011).

[153] J.-Y. Zhang, S.-C. Ji, Z. Chen, L. Zhang, Z.-D. Du, B. Yan, G.-S. Pan, B. Zhao, Y.-J. Deng, H. Zhai, S. Chen, and J.-W. Pan, Collective Dipole Oscillations of a Spin-Orbit Coupled Bose-Einstein Condensate, Phys. Rev. Lett. **109**, 115301 (2012).

[154] P. Wang, Z.-Q. Yu, Z. Fu, J. Miao, L. Huang, S. Chai, H. Zhai, and J. Zhang, Spin-Orbit Coupled Degenerate Fermi Gases, Phys. Rev. Lett. **109**, 095301 (2012).

[155] L. W. Cheuk, A. T. Sommer, Z. Hadzibabic, T. Yefsah, W. S. Bakr, and M. W. Zwierlein, Spin-Injection Spectroscopy of a Spin-Orbit Coupled Fermi Gas, Phys. Rev. Lett. **109**, 095302 (2012).

[156] C. Qu, C. Hamner, M. Gong, C. Zhang, and P. Engels, Observation of *Zitterbewegung* in a spin-orbit-coupled Bose-Einstein condensate, Phys. Rev. A **88**, 021604(R) (2013).

[157] L. Li, C. H. Lee, and J. Gong, Topological Switch for Non-Hermitian Skin Effect in Cold-Atom Systems with Loss, Phys. Rev. Lett. **124**, 250402 (2020).

[158] S. Fölling, S. Trotzky, P. Cheinet, M. Feld, R. Saers, A. Widera, T. Müller, and I. Bloch, Direct observation of second-order atom tunnelling, Nature (London) **448**, 1029 (2007).

[159] Z. Fu, P. Wang, L. Huang, Z. Meng, H. Hu, and J. Zhang, Optical control of a magnetic Feshbach resonance in an ultracold Fermi gas, Phys. Rev. A **88**, 041601(R) (2013).

[160] J. Jie and P. Zhang, Center-of-mass-momentum-dependent interaction between ultracold atoms, Phys. Rev. A **95**, 060701(R) (2017).

[161] F. Qin, J. Jie, W. Yi, and G.-C. Guo, High-momentum tail and universal relations of a Fermi gas near a Raman-dressed Feshbach resonance, Phys. Rev. A **97**, 033610 (2018).

[162] Here Γ is contributed by the $2L$ sites of the cold-atom setup.

[163] Actual experimental lattices are usually bounded except in circuit implementations [175,176], where the wire connectivity is not tied to their physical embedding.

[164] F. Mila and K. P. Schmidt, Strong-coupling expansion and effective Hamiltonians, in *Introduction to Frustrated Magnetism*, edited by C. Lacroix, P. Mendels, and F. Mila, Springer Series in Solid-State Sciences Vol. 164 (Springer, Berlin, 2010), pp. 537–559.

[165] F. M. C. Lacroix and P. Mendels, *Introduction to Frustrated Magnetism*, Springer Series in Solid-State Sciences Vol. 164 (Springer, Berlin, 2011), Chap. 20.

[166] J. J. Sakurai and S. F. Tuan, *Modern Quantum Mechanics* (Addison-Wesley, Reading, MA, 1994), Chap. 5.

[167] J. Zhou and W. Zhang, Fermi polaron in dissipative bath with spin-orbit coupling, Europhys. Lett. **134**, 30004 (2021).

[168] D. Manzano, A short introduction to the Lindblad master equation, AIP Adv. **10**, 025106 (2020).

[169] J.-S. Pan, L. Li, and J. Gong, Point-gap topology with complete bulk-boundary correspondence and anomalous amplification in the Fock space of dissipative quantum systems, Phys. Rev. B **103**, 205425 (2021).

[170] K. Kawabata, T. Numasawa, and S. Ryu, Entanglement phase transition induced by the non-Hermitian skin effect, arXiv:2206.05384.

[171] X.-J. Liu, Z.-X. Liu, and M. Cheng, Manipulating Topological Edge Spins in a One-Dimensional Optical Lattice, Phys. Rev. Lett. **110**, 076401 (2013).

[172] X.-J. Liu, K. T. Law, and T. K. Ng, Realization of 2D Spin-Orbit Interaction and Exotic Topological Orders in Cold Atoms, Phys. Rev. Lett. **112**, 086401 (2014).

[173] J.-S. Pan, X.-J. Liu, W. Zhang, W. Yi, and G.-C. Guo, Topological Superradiant States in a Degenerate Fermi Gas, Phys. Rev. Lett. **115**, 045303 (2015).

[174] J. Fan, X. Zhou, W. Zheng, W. Yi, G. Chen, and S. Jia, Magnetic order in a Fermi gas induced by cavity-field fluctuations, Phys. Rev. A **98**, 043613 (2018).

[175] J. Ningyuan, C. Owens, A. Sommer, D. Schuster, and J. Simon, Time- and Site-Resolved Dynamics in a Topological Circuit, Phys. Rev. X **5**, 021031 (2015).

[176] C. H. Lee, S. Imhof, C. Berger, F. Bayer, J. Brehm, L. W. Molenkamp, T. Kiessling, and R. Thomale, Topolectrical circuits, Commun. Phys. **28**, 1 (2018).